conference papers

Focusing and polarized neutron small-angle scattering spectrometer (SANS-J-II). The challenge of observation over length scales from an ångström to a micrometre

Satoshi Koizumi,[a]* Hiroki Iwase,[a] Jun-ichi Suzuki,[b] Takayuki Oku,[b] Ryuhei Motokawa,[a] Hajime Sasao,[b] Hirokazu Tanaka,[a] Daisuke Yamaguchi,[a] Hirohiko M. Shimizu[b,c] and Takeji Hashimoto[a]

[a]Research Group for Soft Matter and Neutron Scattering, Advanced Science Research Center, Japan Atomic Energy Agency, Tokai, Ibaraki 319-1195, Japan, [b]Neutron Technology Development Research Center, Japan Atomic Energy Agency, Tokai, Ibaraki 319-1195, Japan, and [c]KEK, Tsukuba, Ibaraki, 305-0001, Japan. Correspondence e-mail: koizumi.satoshi@jaea.go.jp

SANS-J (a pinhole small-angle neutron scattering spectrometer at research reactor JRR3, Tokai, Japan) was reconstructed as a focusing and polarized neutron small-angle scattering spectrometer (SANS-J-II). By employing focusing lenses of a biconcave MgF_2 crystal or of a sextupole permanent magnet and a high-resolution photomultiplier, the minimum accessible magnitude of the scattering vector q_{min} was improved from 3×10^{-3} Å^{-1} to an ultra-small-angle scattering (USAS) of 3×10^{-4} Å^{-1}. Compared with a Bonse–Hart double-crystal method, the advantages of focusing USAS are the efficient detection of anisotropic USAS with an area detector, an improvement in q resolution $\Delta q/q$ at conventional magnitudes of the scattering vector $q \sim 10^{-3}$ Å^{-1} and a gain in neutron flux in the conventional q region of $q \sim 10^{-3}$ Å^{-1}.

1. Introduction

A hierarchy of scales is one of the most widespread features of nature, including the structures found in living things (shown schematically in Fig. 1). The cells of plants or animals, the size of which ranges from 100 µm to a few micrometres, contain organelles (such as the nucleolus, mitochondria, chloroplasts and endoplasmic reticulum) of size 1 µm–100 nm. The cell and organelles are enclosed by a plasma membrane composed of lipids, the size of which is about 1 nm. In the membrane and cytoplasm there are a huge number of proteins acting as channels, enzymes or cytoskeleton, among others. We address the question of whether small-angle scattering approaches can be used to investigate such hierarchically ordered systems, covering length scales ranging from micrometres to ångströms.

We have recently developed a small-angle neutron scattering (SANS) instrument to address this question. A focusing and polarized neutron small-angle scattering spectrometer (SANS-J-II) was constructed by adding advanced neutron optical devices to the conventional reactor SANS spectrometer SANS-J at research reactor JRR3, Tokai, Japan (Koizumi *et al.*, 2006). The q range covered by SANS-J is from 10^{-3} Å^{-1} to 0.1 Å^{-1}, where $q = (4\pi/\lambda)\sin(\theta/2)$ is the magnitude of the scattering vector derived from the wavelength λ and the scattering angle θ. To improve the minimum accessible magnitude of the scattering vector q_{min} to an order of 10^{-4} Å^{-1}, the focusing technique plays the most important role. We redesigned the collimator chamber in order to install two focusing lenses: a Halbach-type sextupole permanent magnetic lens (Oku *et al.*, 2004) and a compound refractive lens made from MgF_2 (Choi *et al.*, 2000). The details of the sextupole magnetic lens of SANS-J-II are reported by Oku *et al.* (2007).

By installing high-angle area detectors on SANS-J, we extended the accessible higher q up to 2 Å^{-1}, as reported by Iwase *et al.* (2007). We aim to eliminate or discriminate incoherent scattering from hydrogen by polarization analysis with a supermirror spin analyser on the high-angle detector. After the construction of SANS-J-II, we successfully achieved the widest q region covered by one spectrometer at a reactor site: four orders of magnitude from 10^{-4} Å^{-1} to 2.0 Å^{-1}. If we also use a Bonse–Hart double-crystal USANS spectrometer with grooved perfect crystals and thermal neutrons we can cover a fifth order of magnitude, giving a total q range of 10^{-5} Å^{-1} to 2.0 Å^{-1}. The ability to make observations over such a wide q range will prove useful in the investigation of the structures of various sizes that are encountered in biological systems.

In this paper, we describe the design of the SANS-J-II spectrometer, highlighting the focusing collimation achieved by the combination of a compound refractive lens and an area detector with a greater position resolution of 0.5 mm. Then, by looking at the results of experiments on soft materials, we discuss the advantages of focusing SANS or USANS: a reduction of q_{min} to $q_{min} \sim 10^{-4}$ Å^{-1}, the observation of anisotropic USANS, the improvement of q resolution $\Delta q/q$ and the intensity gain in the conventional q region of $q > 10^{-3}$ Å^{-1}.

2. Spectrometer design

2.1. Pinhole SANS spectrometer (SANS-J)

Since 1991, SANS-J has been operated at the end of a cold neutron guide (C-3-2) with a neutron flux of 1.0×10^8 n cm^{-2} s^{-1} [see Fig. 2(*a*)]. The total spectrometer length (20 m) is symmetrically divided
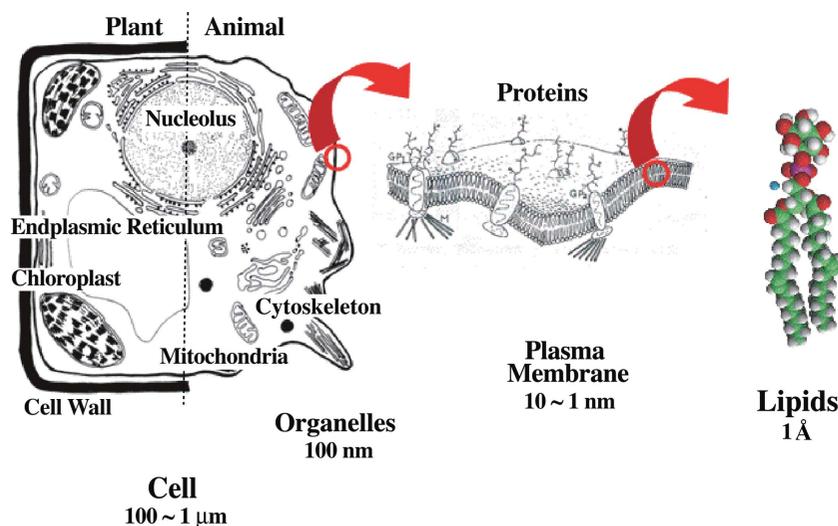
Figure 1
Hierarchical orders in the cell, found over a wide length scale from Å to μm.
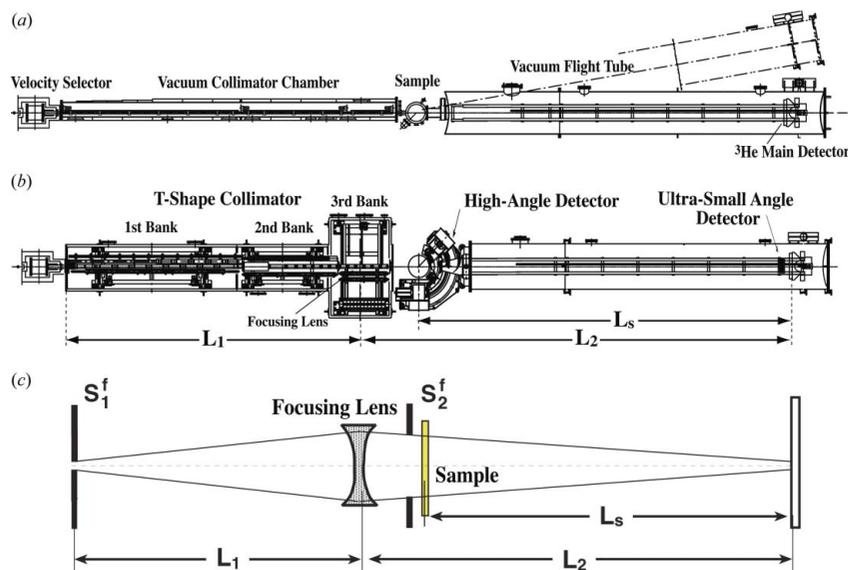

Figure 2
(a) Schematic view for conventional pinhole SANS (SANS-J). (b) Focusing and polarized neutron USAS spectrometer (SANS-J-II), where L_1, L_2 and L_s are distances of first aperture to lens, lens to detector and sample to detector, respectively. (c) Schematic diagram of focusing collimation, where S_1^f and S_2^f indicate slit diameters.

10^5 n cm^{-2} s^{-1} at the sample position. With the shortest camera length (1.3 m) we reach $q = 0.2$ Å^{-1}. Higher q (~0.4 Å^{-1}) can be achieved by tilting the flight tube through an angle of up to 10°.

2.2. Focusing and polarized neutron small-angle scattering spectrometer (SANS-J-II)

During the modification of SANS-J into SANS-J-II, we maintained three important characteristics of the instrument. The total spectrometer length remained 20 m and we kept both the velocity selector and the ^{3}He RISØ-type area detector. Consequently, SANS-J-II is able to cover the conventional SANS q region accessed by SANS-J (3×10^{-3} Å$^{-1} < q < 0.2$ Å^{-1}).

To obtain observations over a wider q range of 10^{-4} Å^{-1} to 2.0 Å^{-1}, we added three items, as shown in Fig. 2(b). A 'T-shaped' collimator with focusing and polarizing devices and a high-resolution area detector in front of the main ^{3}He detector were added in order to achieve USAS of order 10^{-4} Å^{-1} (Koizumi, 2004; Koizumi et al., 2006). A high-angle ^{3}He detector with a spin analyzer was placed at the sample position for high-q observation (Iwase et al., 2007). We completed construction at the end of 2005 and SANS-J-II has been in operation since 2006.

2.2.1. T-shaped collimator. The new T-shaped collimator chamber is designed to enable the installation of focusing and polarizing devices [Fig. 2(b) or see Fig. 2 in Koizumi et al. (2006)]. This collimator chamber (total length 9.37 m) is divided into three banks (4.9 m, 2.63 m and 1.84 m, respectively). The first and second banks (1.26 m width and 0.94 m depth) have horizontally sliding (0.56 m width with four different beamlines) and vertically elevating benches (two stages). By changing bench positions, we can choose a variety of collimations for polarized or unpolarized neutrons. The third collimator bank is made from non-magnetic stainless steel and is wider (2.57 m) in order to install lenses of biconcave MgF$_2$ crystal and a sextupole permanent magnet.

The focusing lens for SANS-J-II is installed at a nearly symmetric position ($L_1 \simeq L_2 \simeq L_s$) in the third bank, just before the sample position [see Fig. 2(c)]. The incident beam is narrowly collimated (first aperture diameter $S_1 \sim 2$ mm) by fourfold beam slits composed of sintered B$_4$C plates with a tapered edge and four ultrasonic motors. The focusing lens effectively collects diverging neutrons after the first aperture and focuses them (second aperture diameter 15–20 mm) on the detector position ($L_s = 9.6$ m).

The magnetic lens requires a highly polarized and narrowly collimated neutron beam at the first aperture. This is because a polarized neutron with spin parallel to the magnetic field of the lens converges (focusing), whereas one with antiparallel spin diverges (defocusing). Thus, just behind the first aperture, we put a short polarizing Fe/Si supermirror (length ~0.15 m) [see Fig. 3 in Koizumi et al. (2006)]. A transmission beam passes through a solenoid coil providing a magnetic guide field (10 Gauss). The 100 mm diameter coil, the inner wall of which is covered by a B$_4$C impregnated rubber sheet, also acts

at the sample position. The collimator and scattering flight tubes are about 10 m in length. Using a disk-type velocity selector (Rasta, 1989) provided by the Central Research Institute in Hungary, the cold neutrons are monochromated with the maximum of the Maxwellian wavelength distribution at $\lambda = 6.5$ Å and $\Delta\lambda/\lambda$ in the range 0.08 to 0.13. In the vacuum flight tube we put a ^{3}He position-sensitive main detector with a diameter of 60 cm and about 5 mm positional resolution. (The detector was provided by RISØ National Laboratory, Denmark.)

In the collimator, we adjust the Ni mirror neutron guides and pinhole diameters (S_1 and S_2), depending on the sample-to-camera length L_s which can vary from 1.3 m to 10 m. Under typical operating conditions for $q_{min} = 3 \times 10^{-3}$ Å^{-1} ($S_1 = 20$ mm, $S_2 = 8$ mm, $L_S = 10$ m and $\lambda = 6.5$ Å), we obtain a beam flux of approximately 1.1 ×

as a shielding tube. At the top of the second collimator bank, we put a two coil Drabkin π-flipper, which is magnetically shielded by rolled μ-metal plates. For general use, without the magnetic lens, we need a polarized neutron beam that is as large as the Ni guide tube (20 mm width $\times$ 50 mm height). So we put longer Fe/Si supermirrors (length ~2.5 m) at two different positions in the first and third collimator banks.

2.2.2. Focusing lens. In the third collimator bank we put two types of focusing lenses, a compound (MgF_2) lens and a Halbach sextupole permanent magnet lens, both of which are designed to focus a neutron beam of $\lambda = 6.5$ Å (maximum of wavelength distribution) on the high-resolution area detector at $L_s = 9.6$ m.

The compound refractive lens (provided by Ohyo Koken Kogyo Co. Ltd, Japan) is made of individual biconcave MgF_2 lenses. We used a NIST-type lens, whose diameter, radius of curvature R and thickness at center are 30 mm, 25 mm and 1 mm, respectively (Choi *et al.*, 2000). We put 70 individual lenses along the beamline to focus neutrons of wavelength $\lambda = 6.5$ Å. The transmission of the compound lens, T_{lens}, is about 50%, which is improved to 65% by cooling the lens to 150 K.

The magnetic lens is characterized by lens power $G = 1.15 \times 10^4$ [T m^{-2}], core diameter 35 mm, total length $L_{mag} = 1.2$ m, external diameter 160 mm and weight 226 kg (Oku *et al.*, 2007). Two solenoid coils for adiabatic spin transportation (0.3 m thickness, providing 1000 Gauss field at the center) are placed just before and after the magnetic lens. The solenoid coils are cooled with water.

2.2.3. Ultra small angle detector. In front of the main ^{3}He detector, we installed a high-resolution area detector (Fig. 3). This is composed of a 5-inch cross-wired position-sensitive photomultiplier tube (R3239, provide by Hamamatsu Photonics Co. Ltd) with a thin sheet of ZnS/^{6}LiF scintillator (0.2 mm thickness). With this assembly, we obtained 0.5 mm positional resolution (Hirota *et al.*, 2005). The assembly is packed in an aluminium vessel, filled with fresh air, which is connected by a flexible plastic tube to guide cables from outside [see Fig. 4 in Koizumi & Suzuki (2006)]. The high-resolution area detector slides into the direct beam position as shown in Fig. 3(*a*). The distance to the sample for the high-resolution area detector is 9.6 m, which is slightly shorter than for the ^{3}He main detector ($L_s = 10.2$ m). During focusing USANS measurements, conventional SANS ($q > 3 \times 10^{-3}$ Å^{-1}) is simultaneously detected by the main ^{3}He area detector, which is located behind the high-resolution area detector. For conventional pinhole SANS ($q > 3 \times 10^{-3}$ Å^{-1}) the high-resolution area detector moves out to an empty space at the bottom left [Fig. 3(*b*)].

2.2.4. Focusing ultra-small-angle scattering. According to the established principle of small-angle scattering (Guinier & Fournet, 1955), q_{min} is given by

$$q_{min} = \frac{2\pi R_f}{\lambda L_s}, \tag{1}$$

where R_f is the beam size (half width at half height) at the detector. To detect ultra-small-angle scattering, we need to observe inside the small area usually masked by a beam stopper. In the case of SANS-J with $L_s = 9.6$ m and $\lambda = 6.5$ Å, at the edge of a 40 mm diameter mask,
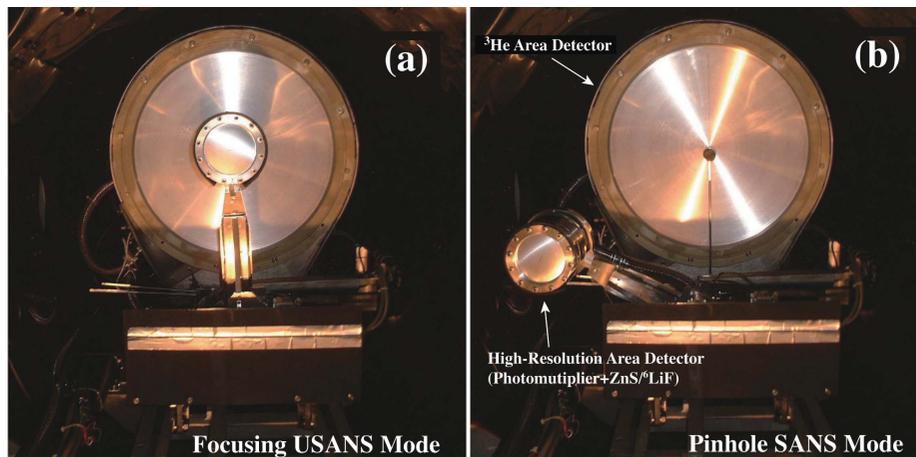

Figure 3
(*a*) Focusing USANS mode with high-resolution area detector located at direct beam position. (*b*) Conventional SANS mode without high-resolution area detector.

$q_{min} = 2 \times 10^{-3}$ Å^{-1}. In order to reach to $q_{min} \sim 10^{-4}$ Å^{-1}, we need $R_f \sim 2$ mm.

A focusing geometry requires an inverse collimation; narrow collimation at the first aperture (diameter S_1) and a wider second aperture (diameter S_2) located just behind the focusing lens or before the sample [see Fig. 2(*c*)]. Compared with the conventional pinhole geometry ($S_1^p = 2$ mm and $S_2^p = 1$ mm), we expect a large intensity gain for the focusing geometry ($S_1^f = 2$ mm and $S_2^f = 20$ mm). The gain factor is given by $g = (S_1^{f2}/S_1^{p2})(S_2^{f2}/S_2^{p2})T_{lens}$ and $g \sim 200$ with $T_{lens} = 0.5$.

A focusing lens reproduces aperture size S_1 at the focusing point when

$$R_f = \frac{1}{2}\frac{L_2}{L_1}S_1. \tag{2}$$

The lens power is characterized by focal length f, where

$$\frac{1}{f} = \frac{1}{L_1} + \frac{1}{L_2}. \tag{3}$$

For the symmetric geometry ($L_1 = L_2$), we obtain $L_1 = L_2 = 2f$.

For the compound lens, f is given by (Eskildsen *et al.*, 1998):

$$f = \frac{R}{\rho b}\frac{1}{\lambda^2 N}, \tag{4}$$

where b, ρ and N are the coherent scattering length, mass density and stack number of the compound lenses, respectively. R determines the mass distribution at the interface of the refractive lens. Note that f is inversely proportional to λ^2.

For the sextupole magnetic lens, on the other hand, f is given by (Oku *et al.*, 2003)

$$f = \frac{h^2}{G\alpha m_n^2}\frac{1}{\lambda^2 L_{mag}}, \tag{5}$$

where h, α and m_n are Planck's constant, the device constant ($\alpha = 5.77$) and the mass of neutron, respectively. The focal length f is inversely proportional to G, which determines the magnetic field gradient along a radial direction in the lens; the magnetic field decreases parabolically from the outside to the center of the lens.

If we compare equations (4) and (5), we find that (i) f changes according to $1/\lambda^2$, which is common for both refractive and magnetic lenses, (ii) the lens power (G) for the magnetic lens is equivalent to 1/

R for the refractive lens and (iii) L_{mag} for the magnetic lens is equivalent to N for the refractive lens. We designed our compound lens and magnetic lenses according to equations (4) and (5), aiming to have the focusing point at $L_s = 9.6$ m with $\lambda = 6.5$ Å.

3. Results and discussion

First we examined R_f, observed at $L_s = 9.6$ m, with both the biconcave compound lens ($N = 70$) and the sextupole permanent magnetic lens. The collimation condition we employed was $S_1^f = 2$ mm and $S_2^f = 20$ mm. Fig. 4 shows R_f as a function of λ, which was detected by the high-resolution area detector. The biconcave MgF_2 lens, focusing unpolarized neutrons, gave a minimum $R_f \sim 1.8$ mm with $\lambda = 6.6$ Å. The sextupole permanent magnetic lens, focusing polarized neutrons (with polarization $P = 0.95$), gave a minimum $R_f \sim 2.3$ mm with $\lambda = 6.8$ Å.

Fig. 5 compares the focused beam profiles obtained with $\lambda = 6.65$ Å, which give the minimum R_f, as shown in Fig. 4. The beam profiles (a), (b) and (c) were obtained using the compound lens for three different wavelength distributions with $\Delta\lambda/\lambda = 0.13$, 0.1 and 0.08, respectively. Profiles (a)–(c) were significantly narrower than the profile (d), obtained by conventional collimation without a focusing lens ($S_1 = 20$ mm and $S_2 = 8$ mm). The steep drop in normalized intensity from 1 to 10^{-5} [marked by (I) in Fig. 5] changes slightly as $\Delta\lambda/\lambda$ becomes smaller. This initial reduction (I) is attributed to chromatic aberration as a result of the wavelength distribution. Chromatic aberration changes to formula R_f (Littrell, 2004): instead of equation (2) we have

$$R_f = \frac{1}{2}\left[S_1 \frac{L_2}{L_1} + S_2 \frac{\Delta\lambda}{\lambda}\left(1 + \frac{L_2}{L_1}\right)\right]. \quad (6)$$

The second term in equation (6) is due to chromatic aberration and is proportional to S_2 and $\Delta\lambda$. If we could use a perfectly monochromatic neutron beam ($\Delta\lambda = 0$), the second term would disappear and the focused beam profile would be rectangular as illustrated in Fig. 5 profile (e). As discussed by Koizumi et al. (2006), a combination of S_1
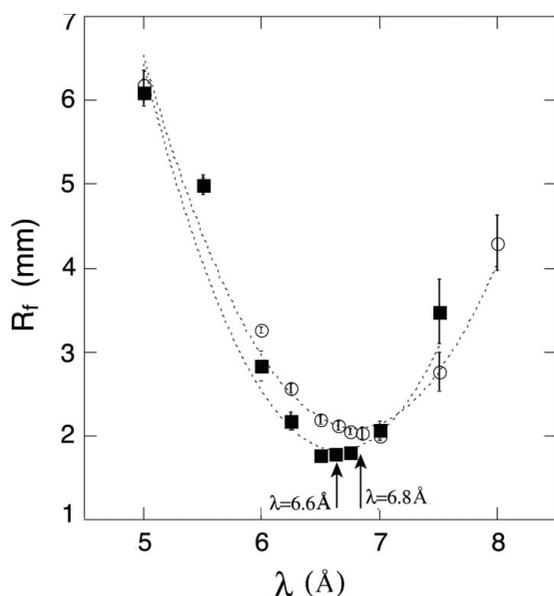
$= 2$ mm with $\Delta\lambda/\lambda = 0.13$ affects R_f in such a way that we are able to obtain a focused beam with a small spot size and high intensity.

At intensities lower than 10^{-5} the profiles (a)–(c) start to fall gradually as q^{-3} [as marked by (II) in Fig. 5]. This fall (II) can be attributed to parasitic scattering of the beam by slit, air, aluminium windows or imperfections of the lens. If we put a vacuum tube in between the collimator and flight tube and remove the aluminium windows, this component (II) decreased by about 50%. As we discussed in Koizumi et al. (2006), this gradual decay (II) is crucial in limiting q_{min}, especially for weak scattering powers with $d\Sigma/d\Omega < 100$ cm^{-1}.

Polarized neutrons with $P = 0.95$ and $\Delta\lambda/\lambda = 0.13$ were also focused by the magnetic lens [Fig. 5 profile (g)]. Similar to (a)–(c), the profile (g) initially decays because of the chromatic aberration effect. However a non-decaying plateau appears at an intensity of 10^{-3}–10^{-5}. This plateau originates from the defocusing of the part of the beam with antiparallel spin. If we focus unpolarized neutrons ($P = 0$) using the magnetic lens, this plateau appears at 10^{-3} [Fig. 5 profile (f)]. The position of this plateau can be estimated by considering the capability of the lens (determined by G, L_{mag}), the core size of the lens and the homogeneity of the neutron beam in the lens. If we assume that the incident neutron is homogeneously diverged after the first aperture, the defocusing plateau is estimated to appear at 9×10^{-4} and 2.3×10^{-5} for $P = 0$ and $P = 0.95$, respectively. To reduce the defocusing plateau to $\sim 10^{-6}$ we need to prepare polarization at more than 0.99 (as indicated in Fig. 5).

The R3932 photomultiplier with $ZnS/^6LiF$ scintillator can discriminate gamma rays, so the noise in the flight tube of SANS-J-II with the beam shutter closed is $\sim 10^{-8}$ (solid line in Fig. 5). An imaging plate with lead shielding (provided by Fuji Film Co. Ltd) and a spatial
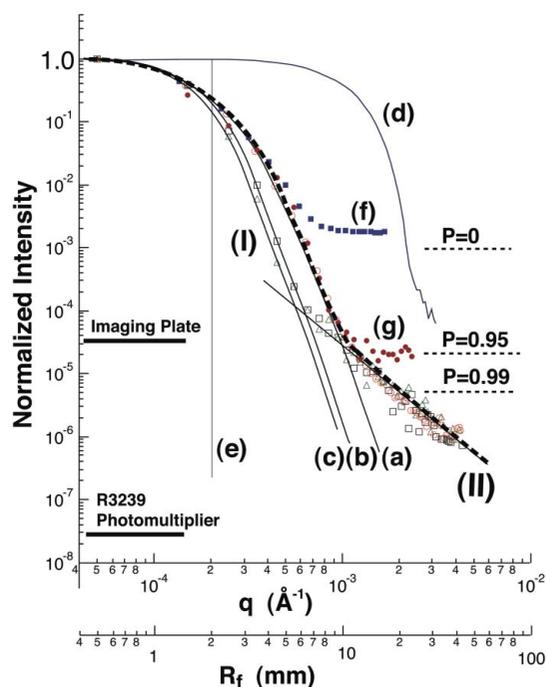

Figure 4
Wavelength dependence of beam size R_f (half width at half height), focused by a compound MgF_2 lens (filled squares) and by a sextupole permanent magnetic lens (open circles).

Figure 5
Focused beam profiles (a)–(c) obtained using compound lenses. Profiles (f) and (g) obtained using magnetic lenses. Profile (d) for a beam without a focusing lens. Profile (e) of ideal focusing without chromatic aberration. Thick solid lines indicate background levels due to electronic noise and γ-rays. Broken lines are background levels estimated for the defocusing of antiparallel neutrons, depending on the polarization P.

resolution <0.1 mm shows the noise at $\sim 10^{-4}$, which is not sufficient for small-angle scattering measurements.

There are three advantages which arise from using focusing collimation. The first advantage is the minimum magnitude of the scattering vector, q_{min}. We estimated the instrument's q resolution $\Delta q/q$ with the direct beam profiles (a) and (d) from Fig. 5. The minimum magnitude of the scattering vector is found when $\Delta q/q = 1$. Using a focused beam shifts q_{min} from the conventional SANS q region to the USANS q region $\sim 10^{-4}$ $\mathring{A}^{-1}$ [indicated by (1) in Fig. 6]. However, due to the gradual decay (II) of the focused beam, q_{min} for focusing USANS strongly depends on the scattering power of the specimen [$\sim d\Sigma/d\Omega$ ($q = 0$)], as demonstrated by Koizumi & Suzuki (2006). For observing anisotropic USANS, the focusing USANS method is superior to the Bonse–Hart double-crystal USANS, whose primary beam is line-shaped, causing a large smearing effect. Fig. 7 shows so-called 'abnormal butterfly scattering' obtained for a polymer film of polystyrene/polyvinylmethyl ether mixture (80/20 by weight) which was sheared at 323 K along a perpendicular direction and quenched at room temperature (Koizumi, 2004; Koizumi & Suzuki, 2006). The abnormal butterfly scattering in the ultra-small-angle q region ($q <$
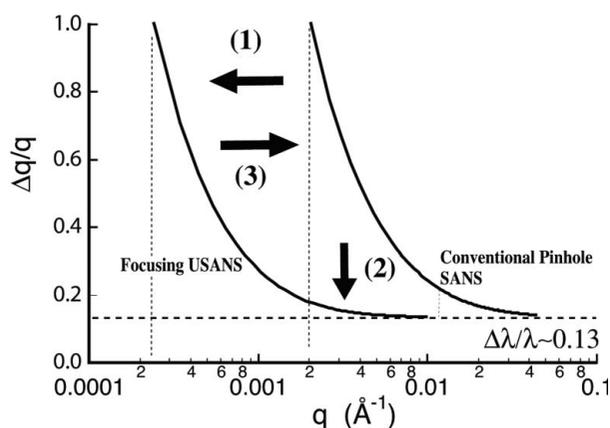
0.001 $\mathring{A}^{-1}$) is successfully detected by the focusing USANS method with a high-resolution area detector.

The second advantage is an improved q resolution in the conventional SANS region of 10^{-3} $\mathring{A}^{-1}$ [as indicated by (2) in Fig. 6]. From $q = 0.002$ to $q = 0.01$ $\mathring{A}^{-1}$, $\Delta q/q$ of focusing USANS is about 0.13, which is determined by $\Delta\lambda/\lambda$, whereas that for conventional SANS is affected by larger R_f and dramatically increases. Fig. 8 shows SANS q profiles for lamellar microdomains of a poly(styrene-block-isoprene)/polystyrene (40/60) mixture (Koizumi et al., 1994). The scattering maximum due to the lamellar lattice factor appears at lower q (as indicated by arrows in Fig. 8) and is much narrower with focusing USANS than with conventional pinhole SANS. The solid lines shown in Fig. 8 are obtained using a one-dimensional paracrystal

Figure 8
SANS q profiles for a binary mixture of polystyrene-block-polyisoprene and polystyrene homopolymer (40/60) obtained by focusing USANS (open circles) and conventional SANS modes (squares). The inset shows a transmission electron microscopy image of the lamellar microdomain.

Figure 6
SANS-J-II q resolution $\Delta q/q$, estimated by using direct beam size R_f for focusing USANS, compared with that for conventional SANS. Thick arrows indicate the advantages of focusing collimation compared with conventional pinhole collimation.
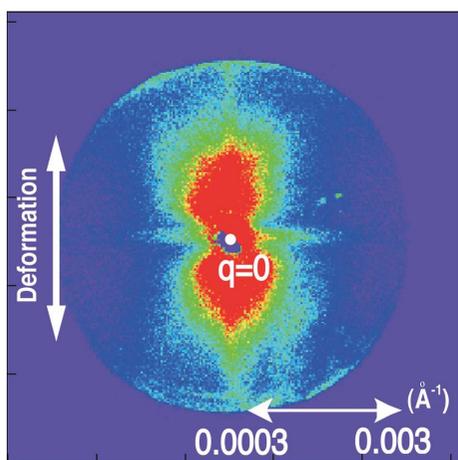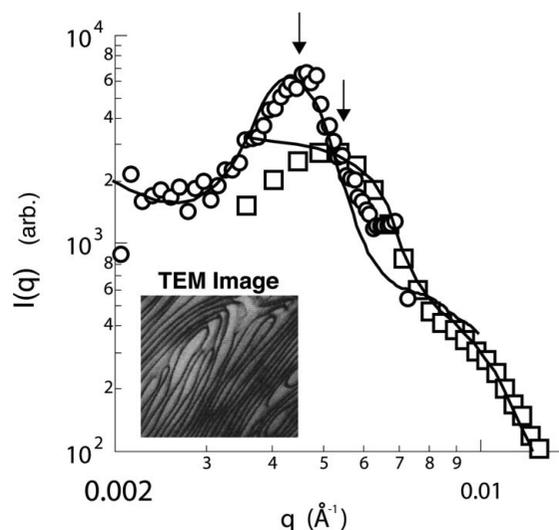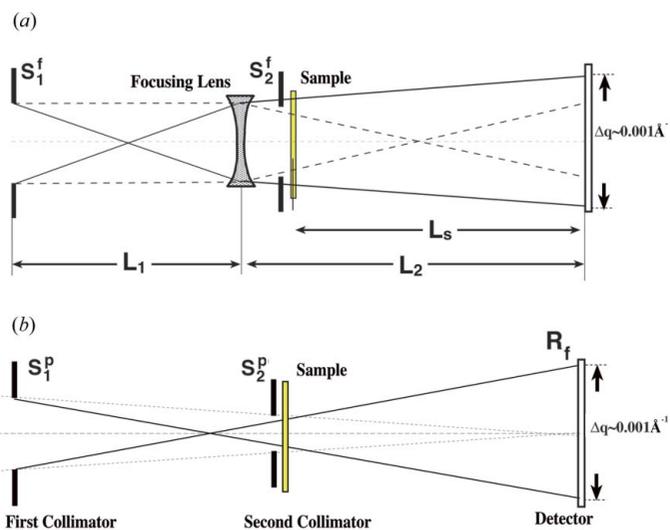

Figure 9
(a) Focusing SANS set-up to measure neutron gain and optimized to provide q resolution comparable with that of (b) conventional SANS.

Figure 7
Butterfly-shaped ultra-small-angle neutron scattering obtained using the focusing USANS mode of SANS-J-II.

model (lamellar spacing d = 1400 Å, thickness of lamellar vesicle = 308 Å, g-factor = 0.15). These reproduce the observed q profiles well after smearing with $\Delta q/q$.

The third advantage [as indicated by (3) in Fig. 6] is the gain in neutron flux obtained with a focusing lens. To demonstrate this we opened the first aperture wider (S_1^f = 20 mm) and reduced the number of lenses (N = 40) [see Fig. 9(a)]. With this combination, we obtained $\Delta q/q$ equivalent to that for conventional SANS [see Fig. 9(b)]. Compared with conventional SANS (S_1^p = 20 mm and S_2^p = 8 mm), we obtained a gain factor of about 3.9 with T_{lens} = 0.63 for the focusing collimation.

4. Summary

A conventional SANS spectrometer (SANS-J) at JRR3 (Tokai, Japan) was successfully reconstructed to a focusing and polarized neutron small-angle scattering spectrometer (SANS-J-II). By using a compound MgF_2 or a sextupole permanent magnetic lens, SANS-J-II is able to reach the magnitude of the scattering vector $q = 10^{-4}$ Å^{-1} in a medium ultra-small-angle scattering, corresponding to a gap in resolution between double-crystal (Bonse–Hart) SANS and conventional pinhole SANS. By using high-angle area detectors with a spin analyser, SANS-J-II is able to reach 2.0 Å^{-1} (Iwase *et al.*, 2007). We have thus achieved observations covering four orders of magnitude in q. The ability to make observations over such a wide q range will prove useful in the investigation of the structures of various sizes that are commonly found in hard, soft and biomaterials.

References

Choi, S.-M., Barker, J. G., Glinka, C. J., Cheng, Y. T. & Gammel, P. L. (2000). *J. Appl. Cryst.* **33**, 793–796.

Eskildsen, M. R., Gammel, P. L., Isaacs, E. D., Detlefs, C., Mortensen, K. & Bishop, D. J. (1998). *Nature (London)*, **391**, 563–566.

Guinier, A. & Fournet, G. (1955). *Small-Angle Neutron Scattering of X-rays*. New York: John Wiley and Sons, Inc.

Hirota, K., Shinohara, T., Ikeda, K., Mishima, K., Adachi, T., Morishima, T., Sato, S., Oku, T., Yamada, S., Sasao, H., Suzuki, J. & Shimizu, H. M. (2005). *Phys. Chem. Chem. Phys.* **7**, 1836–1838.

Iwase, H., Koizumi, S., Suzuki, J., Oku, T., Sasao, H., Tanaka, H., Shimizu, H. M. & Hashimoto, T. (2007). *J. Appl. Cryst.* **40**, s414–s417.

Koizumi, S. (2004). *J. Polym. Sci. Part B*, **42**, 3148–3164.

Koizumi, S., Iwase, H., Suzuki, J., Oku, T., Motokawa, R., Sasao, H., Tanaka, H., Yamaguchi, D., Shimizu, H. M. & Hashimoto, T. (2006). *Physica B*, **385–386**, 1000–1006.

Koizumi, S., Hasegawa, H. & Hashimoto, T. (1994). *Macromolecules*, **27**, 7893–7906.

Koizumi, S. & Suzuki, J. (2006). *J. Appl. Cryst.* **39**, 878–888.

Littrell, K. C. (2004). *Nucl. Instrum. Methods A*, **529**, 22–27.

Oku, T., Suzuki, J., Sasao, H., Adachi, T., Shinohara, T., Ikeda, K., Morishima, T., Sakai, K., Kiyanagi, Y., Furusaka, M. & Shimizu, H. M. (2004). *Nucl. Instrum. Methods A*, **529**, 116–119.

Oku, T., Iwase, H., Shinohara, T., Yamada, S., Hirota, K., Koizumi, S., Suzuki, J., Hashimoto, T. & Shimizu, H. M. (2007). *J. Appl. Cryst.* **40**, s408–s413.

Oku, T., Suzuki, J., Adachi, T., Sakai, K., Ikeda, K., Morishima, T., Kiyanagi, Y., Furusaka, M., Tsuzaki, T. & Shimizu, H. M. (2003). *Proc. ICANS-XVI*, Düsseldorf, May, p. 355.

Rasta, L. (1989). *Phys. B*, **156–157**, 615–618.